Regional Studies in Marine Science 79 (2024) 103852

Contents lists available at ScienceDirect

Regional Studies in Marine Science

journal homepage: www.elsevier.com/locate/rsma

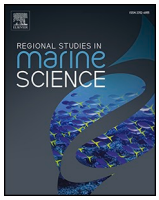

Can automatic measuring replace humans when evaluating a shrimp fishery?

Bent Herrmann [a,b,c,*], Elling Ruud Øye [a], Jonatan Sjølund Dyrstad [a], Anja Helene Alvestad [a]

[a] SINTEF Ocean, Brattørkaia 17C, Trondheim N-7010, Norway
[b] The Arctic University of Norway, UiT, Breivika, Tromsø N-9037, Norway
[c] DTU Aqua, Technical University of Denmark, Hirtshals 9850, Denmark

ARTICLE INFO

Keywords:
Pandalus borealis
Size estimation
Computer vision
Stock structure
Size selectivity
Use-case driven approach
Automatic size measurements

ABSTRACT

Size measurements of fish and crustacean species play a critical role in fishery stock assessments, fishing gear size selectivity studies, and monitoring compliance with fisheries management regulations. One such example is from shrimp fisheries where samples of trawl-caught shrimps are frequently collected and size measured. However, the manual measurement of hundreds of small shrimps per sample is time-consuming and exhausting. Therefore, this study evaluates whether an automatic measuring procedure using off-the-shelf camera technology and a general-purpose artificial intelligence algorithm can replace manual measurements of deep-water shrimp (*Pandalus borealis*). Despite some deviations between manual and automatic measurements for individual shrimps, the automatic method proved sufficiently accurate for stock, gear selectivity and compliance assessment. Furthermore, this study demonstrated how a use-case driven approach can be applied when evaluating whether a new measuring technology can replace an existing.

1. Introduction

Many fisheries face challenges in sustainably exploiting resources, such as overfishing, the capture of undersized individuals, or species composition (Duarte et al., 2020). To mitigate these challenges, fisheries have implemented periodic monitoring of stock sizes, harvest controls, and restrictions on fishing gear types and designs (Melnychuk et al., 2021; Kennelly and Broadhurst, 2021). Increasing demands for accurate data have led to enhanced monitoring efforts (Silva et al., 2020). Accurate estimates of fish population abundance and size distribution are vital for effective fisheries management (Jennings and Polunin, 1997; Jennings and Kaiser, 1998; Pauly et al., 2002). Specifically, size measurements of fish and crustacean species play a critical role in fishery stock assessments, fishing gear size selectivity studies, and monitoring compliance with fisheries management regulations. Specifically, the dynamics of species length distribution is essential for analysing marine population dynamics and making informed management decisions about exploited stocks. First, the data on composition of catches are crucial for stock assessments and management strategies (Jardim et al., 2015). Second, data on the sizes of released and retained species is critical for evaluating size selectivity, helping optimize gear designs for species-specific size discrimination (Wileman et al., 1996; Kennelly and Broadhurst, 2021). Third, regulations may then limit the proportion of undersized individuals in catches, with non-compliance potentially leading to the closure of fishing areas (Larsen et al., 2018b). In such cases the check for compliance is dependent on the size measuring of individuals in the catch.

However, in almost all fisheries, the length estimation of fish and crustacean species is still done manually (Alvarez-Ellacuría et al., 2020). Automation, on the other hand, has the potential to enhance the accuracy, efficiency, and consistency of species measurement, thereby improving the reliability of stock assessment data. Specifically, the developments in artificial intelligence (AI) methods, often combined with computer vision, have significant potential to enhance data collection and processing in marine applications. This potential is highlighted by the formation of the Working Group on Machine Learning Applications in Marine Science (WGMLEARN) by the International Council for the Exploration of the Sea (ICES) in 2019 (ICES, 2019). According to Marrable et al. (2022), deep learning can automate the labour-intensive task of accurately locating the heads and tails of fish, replacing manual methods with computer vision-based algorithms. Monkman et al. (2019) noted that measuring fish length using digital imagery is an expanding field. White et al. (2006) were the first to test this method using computer vision on a fishing vessel (Marrable et al., 2023). Also, for

* Corresponding author at: SINTEF Ocean, Brattørkaia 17C, Trondheim N-7010, Norway.
E-mail address: bent.herrmann@sintef.no (B. Herrmann).

https://doi.org/10.1016/j.rsma.2024.103852
Received 5 August 2024; Received in revised form 22 September 2024; Accepted 28 September 2024
Available online 5 October 2024

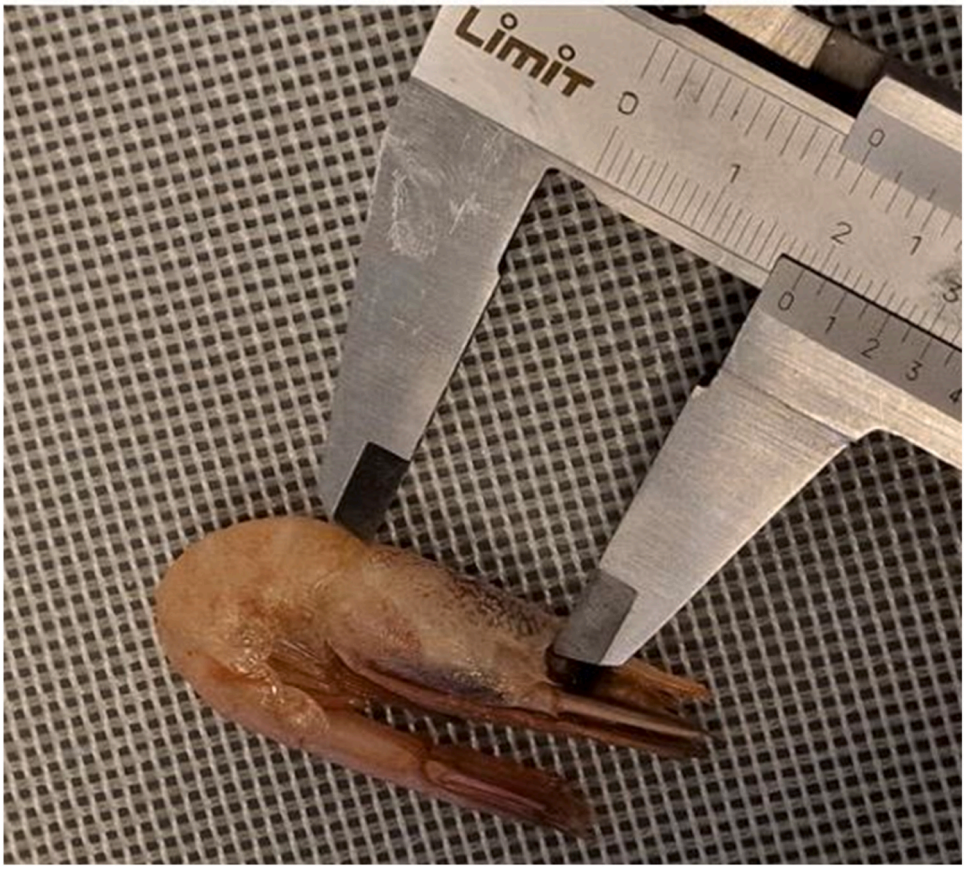

Fig. 1. Measuring the carapace length on a deep-water shrimp with a calliper.

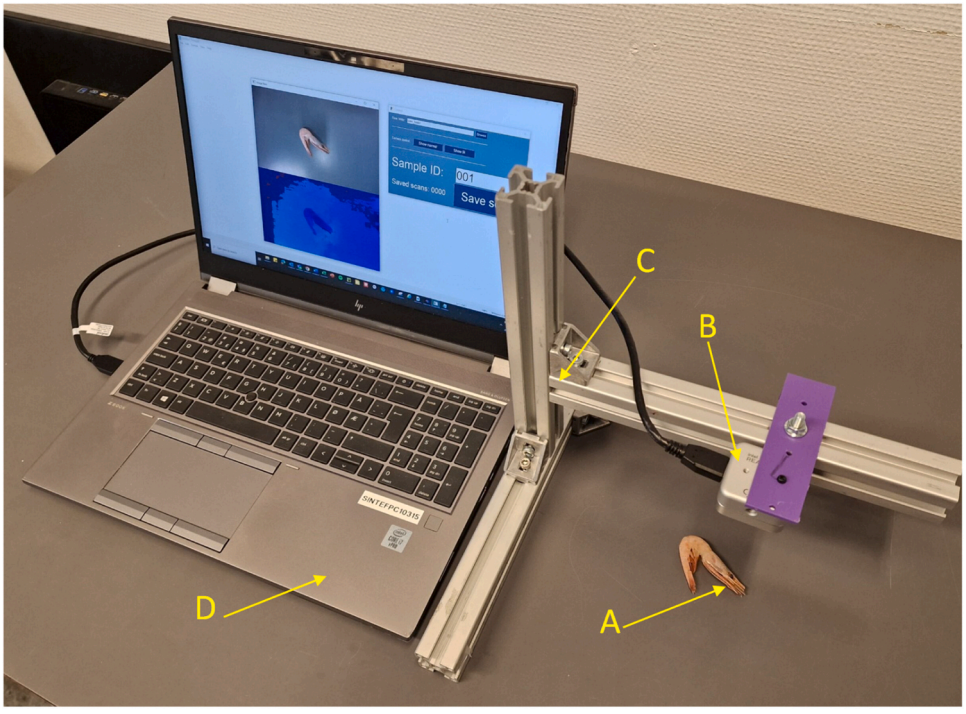

Fig. 2. Acquisition setup for automatic measuring of carapace length on deep-water shrimp. A: deep-water shrimp to be measured. B: Intel Realsense D405 RGB-D camera positioned above the shrimp to be measured. C: compact rack of Rexroth aluminium profiles for camera mount. D: laptop computer controlling acquisition and storing images acquired.

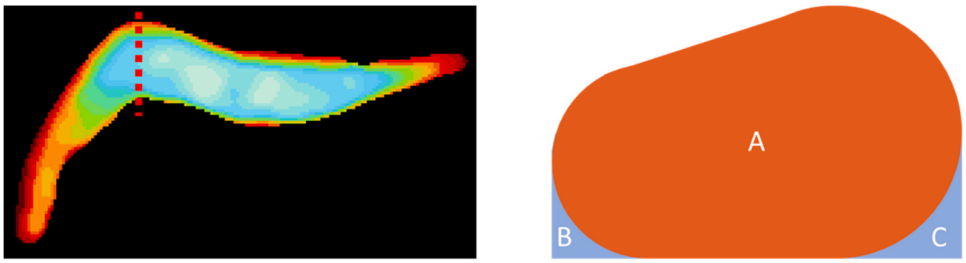

Fig. 3. Depth image of a shrimp (left) and illustration of sections B and C, which are obscured because they are on the side of the shrimp facing away from the camera (right).

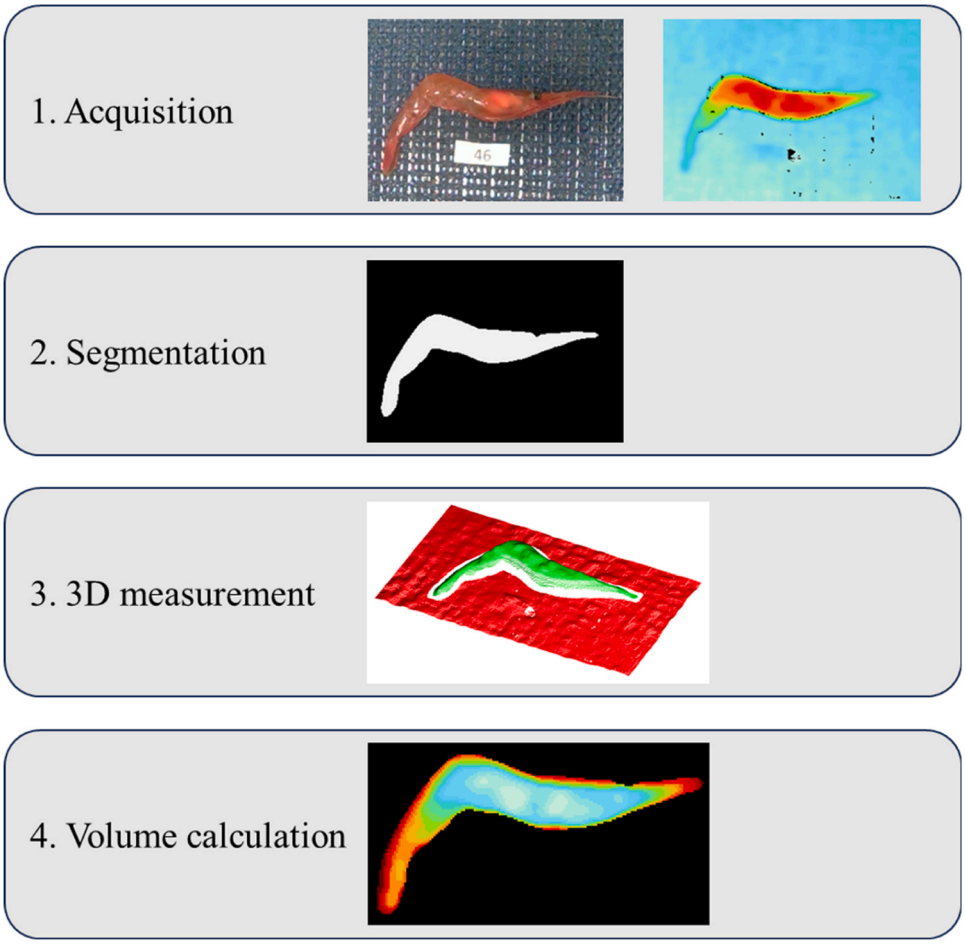

Fig. 4. Steps in the image analyses to obtain value for volume *vr* for a deep-water shrimp.

crustacean species, such as shrimp, automated size measurement using computer vision and AI is increasingly applied, particularly in aquaculture field (Lai et al., 2022; Hashisho et al., 2021). In the context of fisheries stock assessments, Harbitz (2007) explored the use of computer vision for measuring the length of deep-water shrimp (*Pandalus borealis*). The carapace length, often measured with a calliper (Fig. 1), is a standard size metric for shrimp. This manual measurement process can be exhausting and time-consuming, especially when hundreds of individuals across multiple samples need to be recorded. For example, assessing the size selectivity of fishing gear for shrimp typically involves measuring 300–500 individual shrimp collected from each of 8 to 12 trawl hauls per gear configuration tested (Larsen et al., 2017, 2018a).

The deep-water shrimp (also known as the northern shrimp) is a commercially important species that is being harvested by means of demersal trawls along the Norwegian coast since the early 20th century. The fishing of this species expanded to deeper waters off Norway and other countries in the late 1960s (Larsen et al., 2017; Einarsson et al., 2020). Given the economic importance of this species, the current study examines whether the manual measurement of its size by humans, for purposes such as stock assessment, gear size selectivity, and compliance monitoring, can be replaced by an automated measurement system. This system utilizes off-the-shelf camera technology integrated with a general-purpose artificial intelligence algorithm.

2. Materials and methods

2.1. Automatic acquisition method

The purpose of this study is to examine a method based on digital imaging, computer vision, and artificial intelligence to estimate the

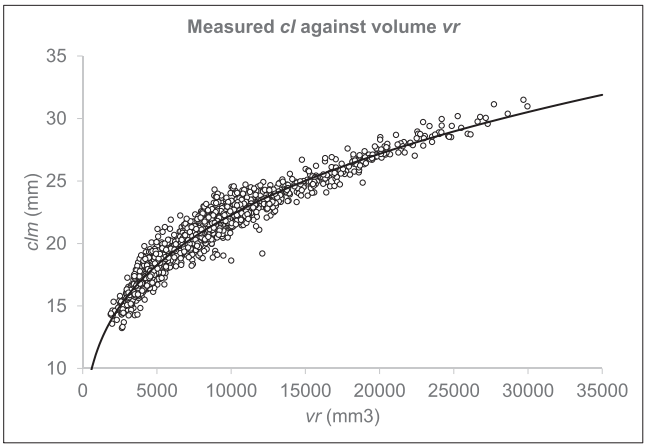

Fig. 5. Measured *cl* (*clm*) versus shrimp volume (*vr*) for individual shrimp (dots) and regression curve based on minimizing Expression (3).

Table 1
Estimated value for parameters *a* and *b* for use in Eq. (2) and fit performance based on minimizing Expression (3).

a	1.5950
b	0.2863
R^2	0.94

carapace length (*cl*) of deep-water shrimp individually. Accurately positioning a shrimp in the imaging setup and reliably detecting both endpoints that define the *cl* simultaneously is challenging. Therefore, our method instead relies on an assumed correlation between the shrimp's volume (*v*) and its *cl*. Assuming the relationship between the shrimp's volume and carapace length follows a power law:

$$cl = a \times v^b \tag{1}$$

Our method involves an acquisition setup with a low-cost 3D camera positioned above the shrimp, which is laid on its side for measurement (Fig. 2). In Eq. (1), a and b are species-specific parameters that need to be known prior or estimated as part of the acquisition process.

Specifically, the camera used for imaging was an Intel Realsense D405 RGB-D camera. This is a low-cost stereo camera that differs from most other RGB-D cameras in this price range due to its ability to capture 3D information at short range. While most other RGB-D cameras have an ideal minimum range of 30 to 60 cm, the Realsense D405 can capture 3D information at distances as close as 7 cm, making it suitable for scanning small objects such as shrimp. The camera uses two IR cameras for stereo matching and an image signal processor to enhance the RGB data from the depth sensor, resulting in an output that combines matching colour and depth.

The camera was mounted on a compact rack of Rexroth aluminium profiles, ensuring that each sample could be positioned at approximately the same distance from the camera. During data collection, the Realsense camera was connected to a computer running a user interface that stored each sample with an ID tag, along with raw colour and depth information.

However, the acquisition setup (Fig. 2) used does not provide the volume *v* required to use Eq. (1) to estimate *cl*, as the side of the shrimp facing away from the camera is obscured (Fig. 3).

Due to the challenge posed by the obscured side of the shrimp, we did not use Eq. (1). Instead, we assumed that the volume resulting from this, denoted as *vr*, has a similar relationship to *cl* as the original volume *v*:

$$cla = a \times vr^b \tag{2}$$

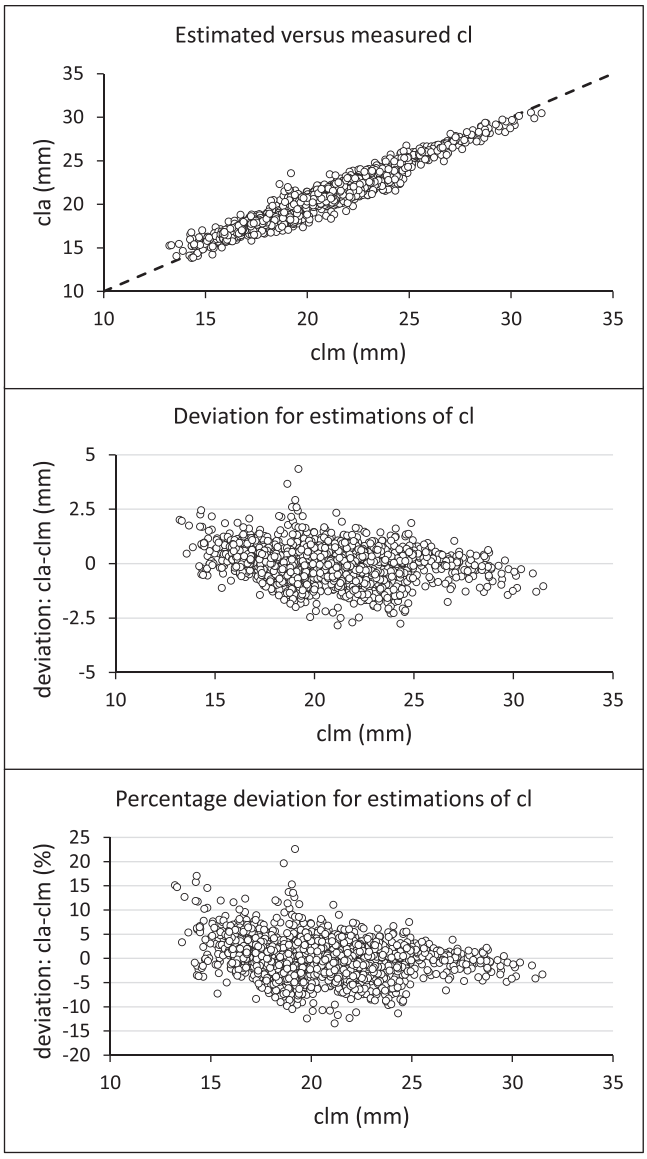

Fig. 6. Estimated *cl-values* (*cla*) versus manual measured *cl-values* (*clm*) (upper panel) and deviations between estimated and measured *cl-values* (centre and lower panel).

Table 2
Mean deviations between estimated and manually measured cl values and the standard deviations (SD).

	Mean	SD
Deviation in cl (mm)	2.31E−4	0.72
Absolute deviation in cl (mm)	0.55	0.47
Deviation in cl (%)	0.14	3.64
Absolute deviation in cl (%)	2.73	2.41

Where we introduced *cla* to represent *cl* in our automatic method. The value of the parameters *a* and *b* in Eq. (2) must be determined before applying our automatic method. The first step, however, is to acquire *vr* using the setup depicted in Fig. 2, which involves the image analysis described below (Section 2.2).

2.2 Image analysis Using the acquisition method described above (Fig. 2), both the colour image and the depth image for each sampled shrimp were utilized for the image analysis. The analysis can be divided into four steps (Fig. 4):

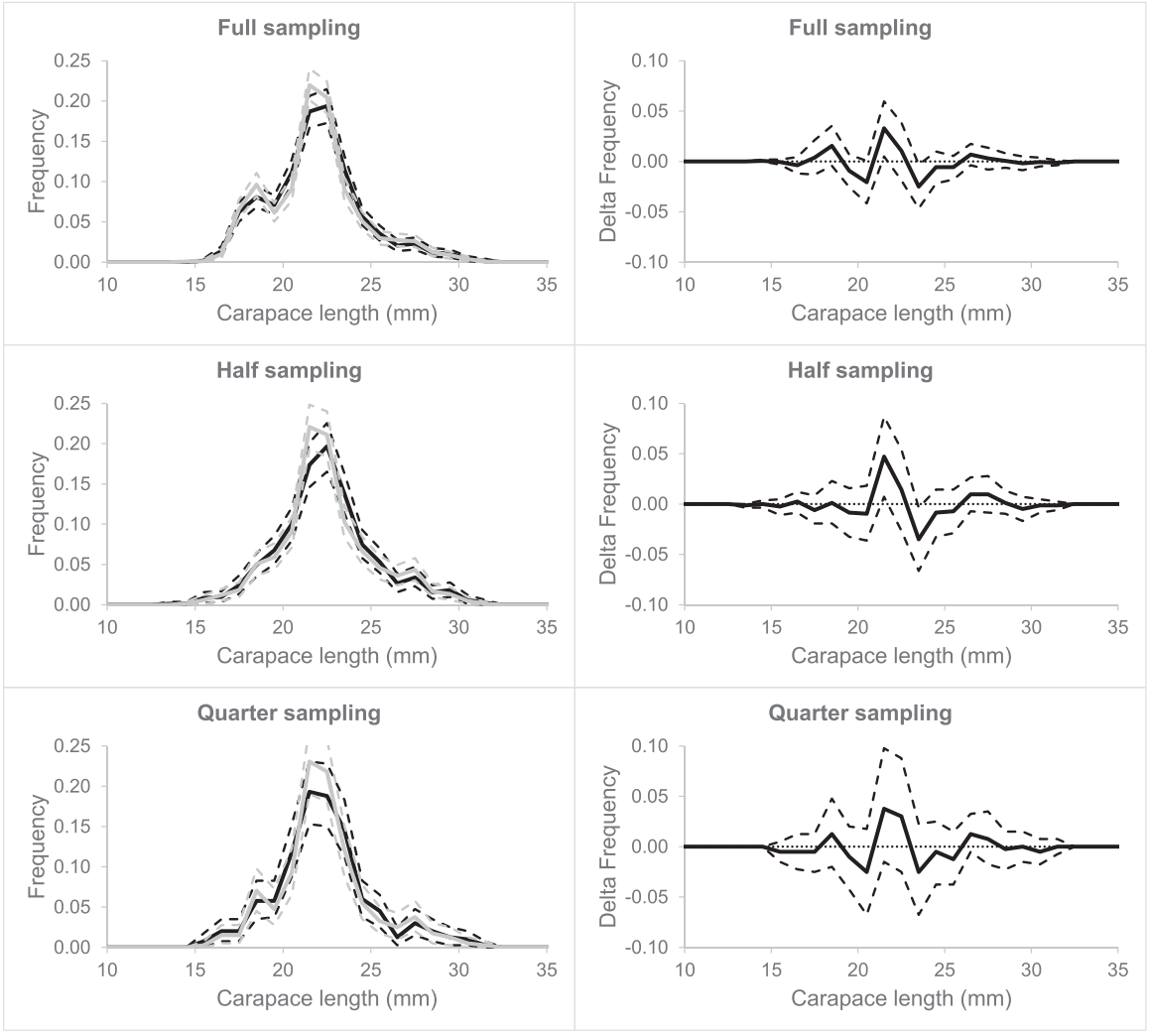

Fig. 7. Population size frequencies based on manual measuring (black curves) and automatic measuring (grey curves) for the entire shrimp data set at three different sampling levels (left column). The right column shows the delta between frequencies (automatic measuring - manual measuring). Dashed curves represent 95 % confidence limits.

1.1. *Acquisition*: Both colour and depth are obtained from the camera.
1.2. *Segmentation*: The object of interest is segmented pixelwise from the background.
1.3. *3D measurement*: The 3D position of each pixel in the depth image is calculated.
1.4. *Volume calculation*: The volume *vr* of the segmented object is calculated based on the 3D measurements.

For the segmentation step (Step 2 in Fig. 4) that separates the shrimp object from the background in the image, our approach utilized the colour image to identify which pixels contained the sample shrimp and which contained the background. We employed the Segment Anything Model (SAM) from Meta AI (https://segment-anything.com) for this purpose. SAM analyses the image and provides segmentations of objects within it. To execute this segmentation task, we utilized a small set of points at the image's edges to help SAM detect the background. Subsequently, the shrimp segmentation was achieved by extracting the largest mask in the centre of the image that did not overlap with the already segmented background. This segmentation method assumes the presence of a single sample per image, positioned in the centre. While various other segmentation strategies are applicable for this task, we opted for SAM primarily due to its robustness. Implementing simpler background detection algorithms based on colour would have required greater control over the background lighting, which was not feasible for use aboard a fishing vessel.

For the 3D measurement step (Step 3 in Fig. 4), the two segmentation masks (background and sample object) were utilized on the depth image. By utilizing the intrinsic properties of the depth camera and the depth values within each segmentation mask, point clouds were computed for both the background and the sample. A RANSAC plane segmentation algorithm (Fischler and Bolles, 1981) was then implemented on the background point cloud to identify a plane and establish a coordinate system aligned with the table on which the shrimp was positioned. Subsequently, the point cloud of the sample was transformed into this coordinate system. The transformation ensured that the z-axis of the point cloud pointed upwards in a perpendicular direction from the plane, while the x- and y-axes were parallel to the table, with the origin located at the centre of the plane.

For the Volume calculation step (Step 4 in Fig. 4), a height map was created from the aligned point cloud of the sample object. The height map had a grid resolution of 0.5 mm, where each square that contained one or more points from the sample point cloud was assigned the point's z-value (or median z-value if multiple points resided within the same grid square). Subsequently, a median filter was employed on the height map, along with an interpolation algorithm to fill in missing grid squares. The area of each sample could then be determined by summing

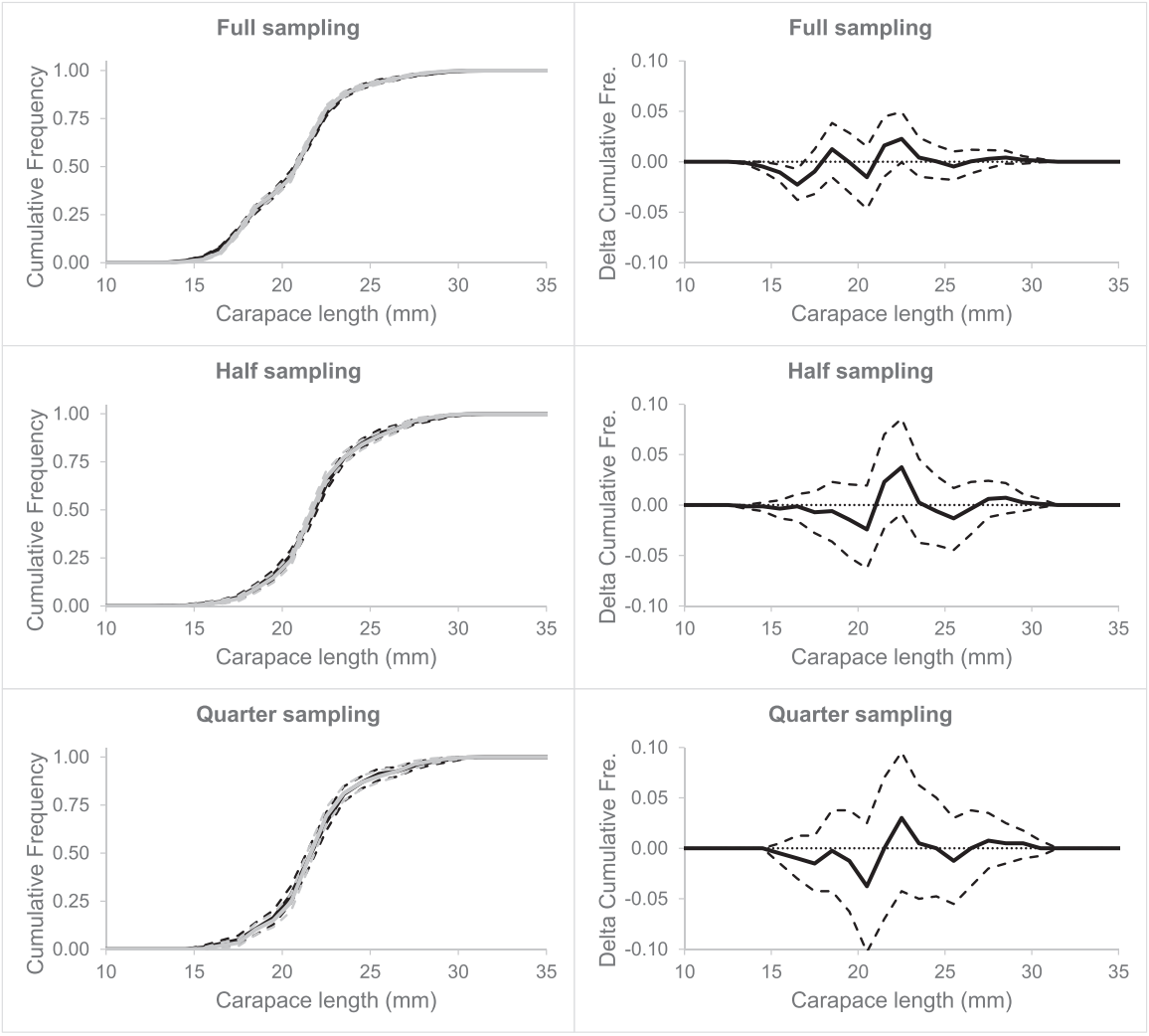

Fig. 8. Cumulative population size frequencies based on manual measuring (black curves) and automatic measuring (grey curves) for the shrimp at three different sampling levels (left column). The right column shows the delta between cumulative frequencies (automatic measuring - manual measuring). Dashed curves represent 95 % confidence limits.

the area of grid squares overlapping the sample, while the volume was calculated by summing the volume of these grid squares. This process resulted in obtaining the value for the sample volume *vr*, which is used to automatically estimate the carapace length of the shrimp *cla* using Eq. (2).

2.2. Data collection

Data sampling was conducted during several hauls on a research cruise with the trawler "Helmer Hanssen" (63.8 m LOA and 4080 HP) in the Barents Sea in February 2023. The fishing trials were performed using a Campelen 1800# trawl constructed entirely of 80–40 mm diamond meshes made of 2 mm polyethylene (PE) twine. The trawl doors utilized were Thyborøn T2 type, measuring 6.5 m^2 and weighing 2200 kg. The design incorporated 40 m double sweeps and a 19.2 m long rockhopper gear composed of three sections with 46 cm rubber discs. Additionally, the trawl had a Nordmøre grid section like the one employed in the Norwegian coastal fleet for targeting shrimp. The stainless steel Nordmøre grid measured 1510 mm in height and 1330 mm in width, angled at 45 ± 2.5° while fishing. The Nordmøre grid had a mean ± SD bar spacing of 18.8 ± 0.4 mm, and the escape exit on the top panel was a 35-mesh long and 70-mesh wide triangle. A small-mesh cover (mean ± SD mesh size 18.9 ± 1.2 mm) was installed over the escape exit to collect escaping shrimps ahead of the grid. To capture the shrimps passing through the grid, the codend included a small, low-hanging, inner net mesh (mean ± SD mesh size 18.5 ± 0.9 mm) to prevent shrimp from escaping. Samples of shrimp were collected from the codend.

For each of the sampled shrimp *i*, the carapace length was measured with a calliper, as shown in Fig. 1, to obtain a clm_i value (manually measured carapace length by a human). The same shrimp was then placed in the image acquisition scene (Fig. 2) to obtain corresponding image data, which ultimately led to a cla_i value for the automatic measurement of the carapace length of the shrimp by using image analysis steps, first obtaining the volume vr_i (Fig. 3).

2.3. Estimation of model parameters

To use our automatic method, the values for the parameters *a* and *b* in Eq. (2) need to be established beforehand. For practical purposes in this study, we used the collected data to determine the values for these parameters based on our corresponding values for clm_i and vs_i, minimizing the sum of the squares of the residuals between the *N* pairs of *vr* and *clm* with respect to *a* and *b*:

$$\sum_{i=1}^{N} (clm_i - a \times vr_i^b)^2 \quad (3)$$

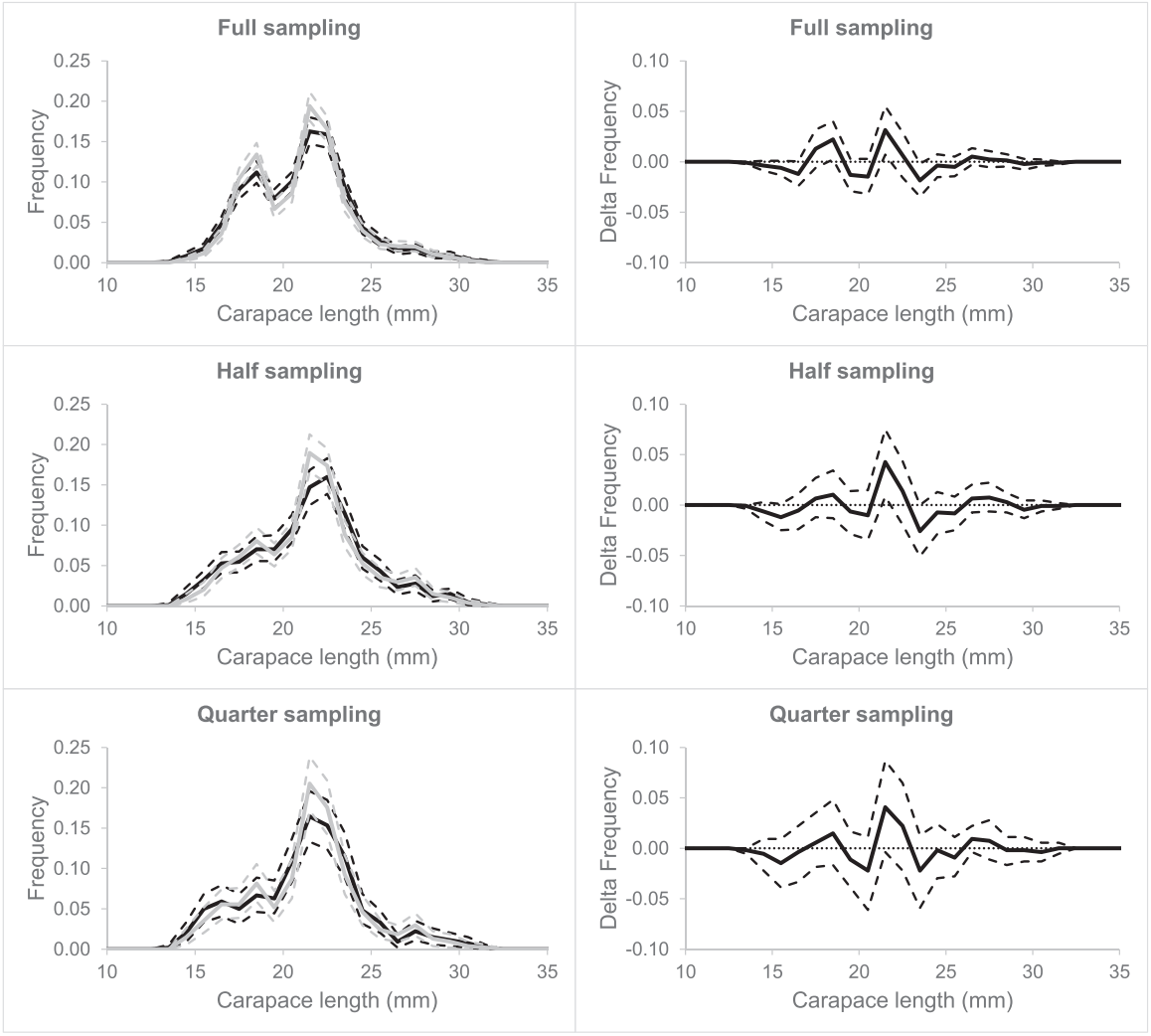

Fig. 9. Population size frequencies based on manual measuring (black curves) and automatic measuring (grey curves) for the simulated retained population using a 35 mm diamond mesh codend. Results are provided for three different sampling levels. The right column shows the delta between frequencies (automatic measuring - manual measuring). Dashed curves represent 95 % confidence limits.

2.4. Data set for performance evaluation

Based on the data collection (Section 2.3) and the established values for parameters *a* and *b* in Eq. (2) (described in Section 2.4), we applied image analysis (Section 2.2) to each of the sampled shrimp. This provided us with the manually measured carapace length by humans clm_i and the automatically measured carapace length cla_i. Thus, our basic dataset consists of paired values (*clm, cla*) for assessing whether the automatic measurement of shrimp carapace length could replace manual measurement by humans using a calliper. The two datasets, based on manual and automatic measurements, are hereafter referred to as the *Mdata* and *Adata* sets, respectively. Comparing results from the *Mdata* and *Adata* sets forms the basis for evaluating whether automatic measurement can replace manual measurement by humans for use in stock assessment, fishing gear size selectivity estimation, and management performance measures.

2.5. Evaluation based on single shrimp measurements

The evaluation on a single shrimp basis was based on comparing the paired values of (*clm, cla*). A preliminary assessment of performance can be obtained by plotting *cla* against *clm* for all measured shrimp and inspecting how much these data points deviate from a line with a slope of 1.0 and an intercept of 0.0. Furthermore, the deviation (in mm and %) between the *clm* and *cla* values can be plotted against the *clm* value. Additionally, the mean and standard deviation (SD) can be calculated based on the sampled data for the deviation between the individual *cla* and *clm* values, as well as for their absolute (unsigned) deviations.

2.6. Evaluation for stock assessment

For stock assessment purposes we based the evaluation on estimated population size structure using 1 mm wide size classes *cl*. The *Mdata* and *Adata* sets were transformed into count numbers n_{cl} (nm_{cl} and na_{cl} respectively) for each *cl*:

$$\begin{aligned} nm_{cl} &= \sum_{i=1}^{N} eq(cl, clm_i) \\ na_{cl} &= \sum_{i=1}^{N} eq(cl, cla_i) \\ &\quad with \\ eq(x,y) &= \begin{cases} 0, \&x \neq y \\ 1, \&x = y \end{cases} \end{aligned} \tag{4}$$

Where N is the number shrimp in the *Mdata* and *Adata* sets. Based on this type of count data (4), a population sample is often described by the length frequency density distribution Dn_{cl} and/or the cumulative length

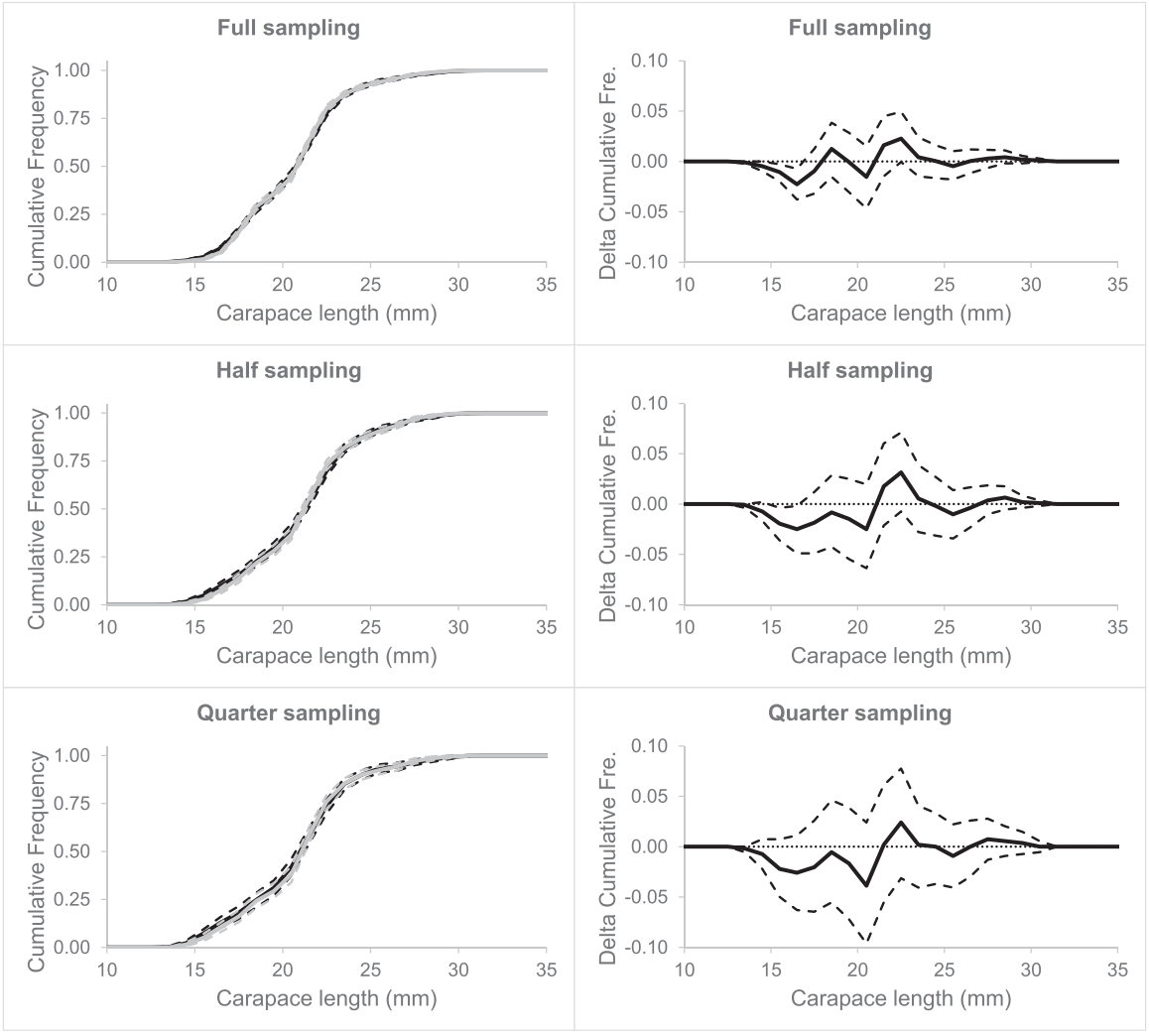

Fig. 10. Cumulative population size frequencies based on manual measuring (black curves) and automatic measuring (grey curves) for the simulated retained population using a 35 mm diamond mesh codend. Results are provided for three different sampling levels. The right column shows the delta between cumulative frequencies (automatic measuring - manual measuring). Dashed curves represent 95 % confidence limits.

Table 3
AIC values for model fits for covered gear experiments. Lowest AIC is indicated in bold, and reflects the model used for each gear configuration and sampling level.

Gear configuration	model	Full sampling		Half sampling		Quarter sampling	
		Human	Auto.	Human	Auto.	Human	Auto.
Nordmøre grid + codend	logistic	1932.3	1975.9	841.3	851.4	**429.5**	**431.5**
Nordmøre grid + codend	dlogistic	**1908.3**	**1967.7**	**819.3**	**835.0**	429.6	433.1
Codend	logistic	**1753.0**	**1800.2**	**670.4**	**672.8**	**415.5**	421.3
Codend	dlogistic	1755.8	1804.5	674.1	675.2	419.8	**419.8**

frequency density distribution CDn_{CL} (Einarsson et al., 2020; Mytilineou et al., 2020). Therefore, we used these two population size structure descriptors in the evaluation for stock assessment purposes. Dn_{cl} quantifies the proportion of individuals within each size class *cl* relative to the total, whereas CDn_{CL} quantifies the cumulative proportion of the total population of shrimp for and up to a given carapace length class *CL*:

$$Dn_{cl} = \frac{n_{cl}}{\sum_{cl} n_{cl}}$$
$$CDn_{CL} = \frac{\sum_{cl=0}^{CL} n_{cl}}{\sum_{cl} n_{cl}} \quad (5)$$

Given that there are *N* shrimps in a sample, where each is measured for length, uncertainties for the sample's Dn_{cl} and CDn_{CL} are obtained based on bootstrapping using 1000 repetitions by resampling *N* individuals with replacement from the sample in each repetition. In each repetition, Eq. (4) and (5) are then applied to obtain a population of 1000 results for Dn_{cl} and CDn_{CL}. From these populations of results,

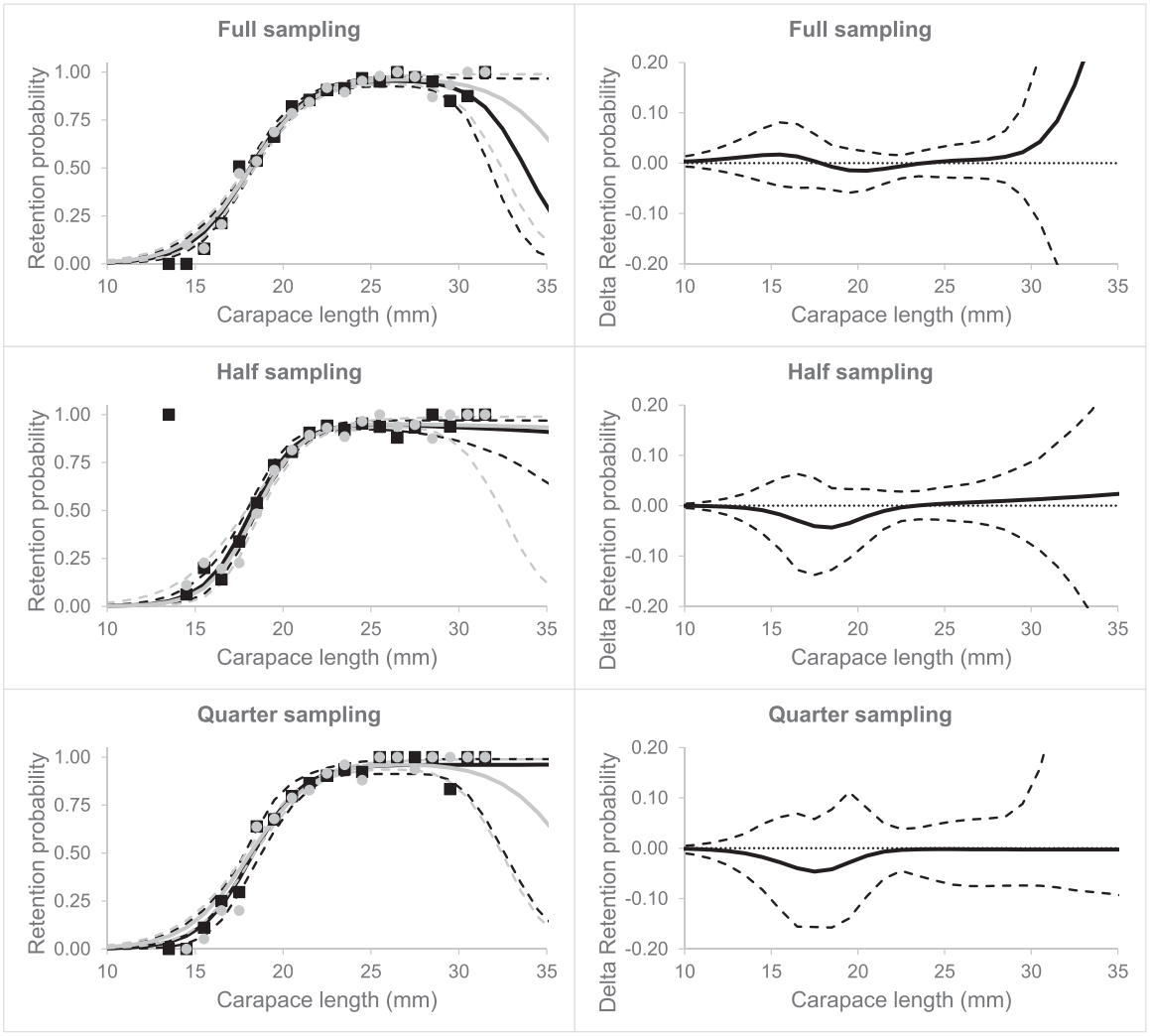

Fig. 11. Covered gear size selection data and curves (left) for a Nordmøre grid followed by a codend for manual data acquisition (black) and automatic acquisition (grey) at three sampling levels. Dots represent the experimental retention rates. Full curves represent the estimated size selection curves, while dashed curves represent the CIs for the size selection curves. The right column shows the delta curves (solid lines) with CIs (dashed lines) between size selection curves obtained using the automatic and manual data acquisition methods.

Efron 95 % percentile confidence intervals (CIs) are obtained (Efron, 1982). This procedure for assessing values for Dn_{cl} and CDn_{CL} with CI's is applied both for the *Mdata* and *Adata* sets to enable comparison regarding application of the automatic method for stock assessment purposes. Specifically, the size-dependent results with CIs are plotted together. Further, to quantify the difference in results between the *Mdata* and *Adata* sets for the length frequency Dn_{cl} and cumulative length frequency CDn_{CL}, the deltas were estimated as follows:

$$\begin{aligned} \Delta Dn_{cl} &= Dna_{cl} - Dnm_{cl} \\ \Delta CDn_{CL} &= CDna_{CL} - CDnm_{CL} \end{aligned} \quad (6)$$

Where Dnm_{cl} and Dna_{cl} are the values for Dn_{cl} for the *Mdata* and *Adata* sets, respectively. The same notation is also used for the CDn_{CL} delta. The CIs for ΔCDn_{CL} and ΔCDn_{CL} were obtained based on the two bootstrap population results for *Mdata* and *Adata* sets, following the procedure for bootstrap calculus described in Herrmann et al. (2018). If all size classes (*cl* and *CL*) contain the value 0.0 inside the CIs for the deltas, no significant difference between the human-based and automatic methods for stock assessment purposes was found.

The procedure described above was applied separately on the full datasets (*Mdata* and *Adata*), the half of the datasets and one-quarter of the datasets to get an impression of whether sample size affects the difference in performance between the *Adata* and *Mdata* sets. Furthermore, these three different sampling levels of data from the paired *Mdata* and *Adata* sets were used as entry data to simulate similar datasets that would be obtained with a size selective fishing gear fishing operating on the entry population. These datasets were simulated using the size selection curve for a Nordmøre grid with 19 mm bar spacing followed by a 35 mm diamond mesh codend (Larsen et al., 2017), as this is the mandatory size selection system for vessels targeting deep-water shrimps in northern Norwegian waters (Norwegian Directorate of Fisheries, 2011). Therefore, we used the size selection curve obtained by Larsen et al. (2017) for the deep-water shrimp for this selective system. The size selection curve *r(cl)* quantifies the probability [0.0; 1.0] that a shrimp entering gear will be retained dependent on its carapace length. Specifically, for each shrimp *i* with a clm_i and cla_i value, we used the clm_i in a stochastic simulation to estimate whether it would be retained or released based on its *clm* value, using the expected mean retention probability *r(clm)*. A random number *z* was then drawn in interval [0.0;1.0]. If $z < r(clm)$, then the shrimp is simulated to be retained, and the *clm* and *cla* values added to the retained fractions. Otherwise, the specific shrimp is simulated to be released and is not considered in the evaluation. The resulting simulated retained population of shrimp was then used to estimate Dn_{cl} and CDn_{CL} for the *Mdata* and *Adata* sets for

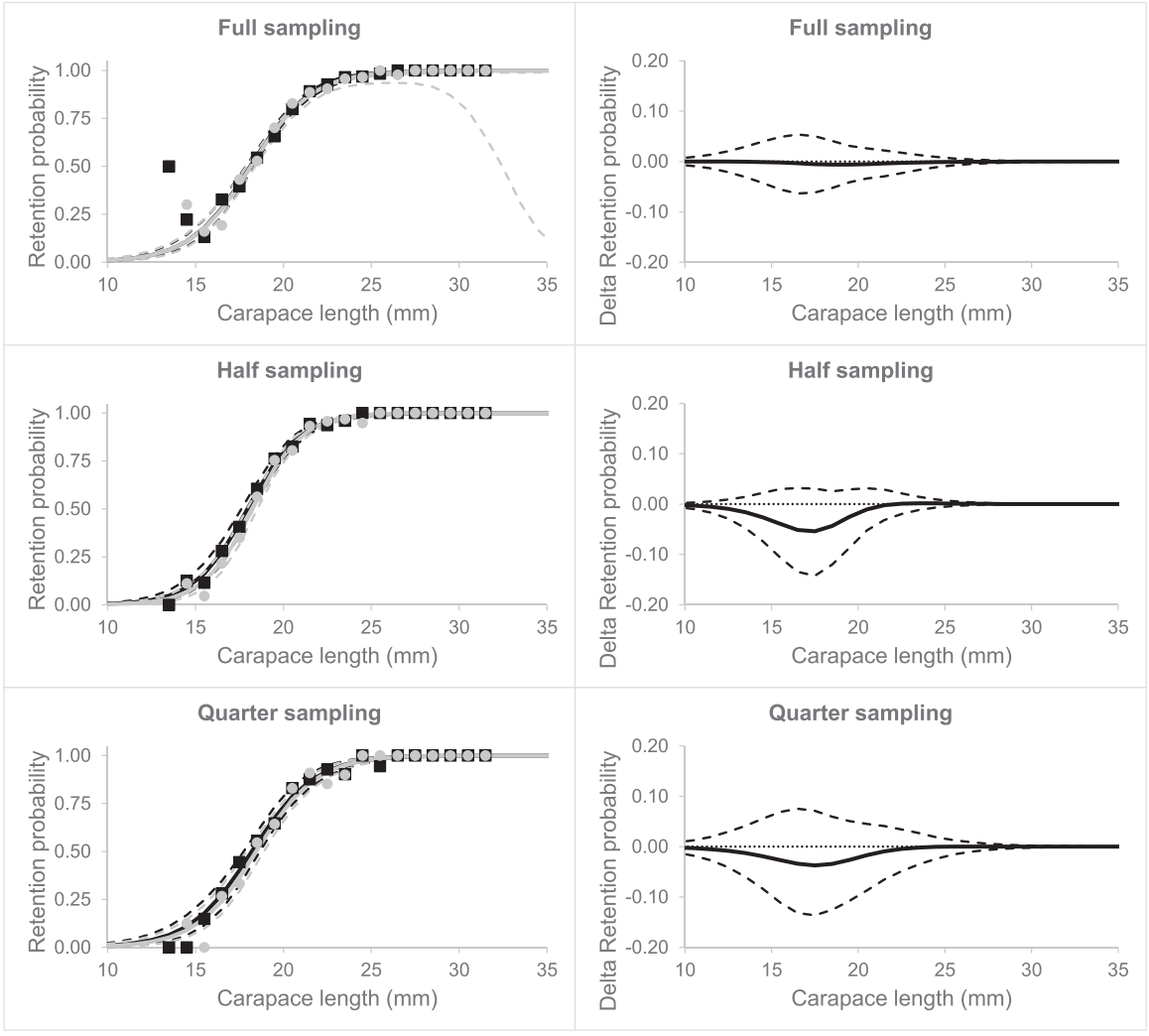

Fig. 12. Covered gear size selection data and curves (left) for a 35 mm diamond mesh codend for manual data acquisition (black) and automatic acquisition (grey) at three sampling levels. Dots represent the experimental retention rates. Full curves represent the estimated size selection curves, while dashed curves represent the CIs for the size selection curves. The right column shows the delta curves (solid lines) with CIs (dashed lines) between size selection curves obtained using the automatic and manual data acquisition methods.

Table 4
AIC values for model fits for paired gear experiments. Lowest AIC is indicated in bold, and reflects the model used for each gear configuration and sampling level.

Gear configuration	model	Full sampling		Half sampling		Quarter sampling	
		Human	Auto.	Human	Auto.	Human	Auto.
Nordmøre grid + codend	logistic	**5037.5**	**5060.5**	**2546.8**	**2552.2**	**1238.3**	**1237.4**
Nordmøre grid + codend	dlogistic	5043.5	5066.5	2552.4	2557.8	1244.3	1243.4
Codend	logistic	**5103.7**	**5108.3**	**2617.6**	**2615.7**	**1256.1**	**1256.9**
Codend	dlogistic	5108.4	5113.2	2623.5	2621.5	1260.8	1262.4

retained population at full, half, and quarter set sizes. Furthermore, the delta values between *Mdata* and *Adata* sets were evaluated according to equation (6).

2.7. Evaluation for fishing gear size selectivity

The covered gear and paired gear method are the two main data collection methods used when experimentally obtaining data for estimating absolute size selectivity of a fishing gear (Wileman et al., 1996; Grimaldo et al., 2016). Absolute size selection quantifies the length dependent probability that a shrimp will be retained by the fishing gear, given that it enters the gear (Wileman et al., 1996). In case of the shrimp, the *cl* value is used for measure of length.

With the covered gear method, both the retained and released fractions of the shrimp are sampled. This is done by having a small mesh net surrounding the fishing gear to collect those individuals escaping. In the case of paired gear method, a small mesh net is towed parallel to the fishing gear to sample an estimate of the population of shrimp entering the fishing gear (Wileman et al., 1996). In the simplest case, size selectivity is estimated at the haul level, and we simplify the assessment of the automatic measuring method to this level. For the covered gear method, let nr_{cl} and ne_{cl} represent the number of shrimps in length class cl being respectively retained in the gear and released through it (collected in the small mesh cover net surrounding it). The parameters ν for the size selectivity curve model $r(cl,\nu)$ are then obtained by maximum likelihood estimation (MLE) by minimizing (Wileman et al.,

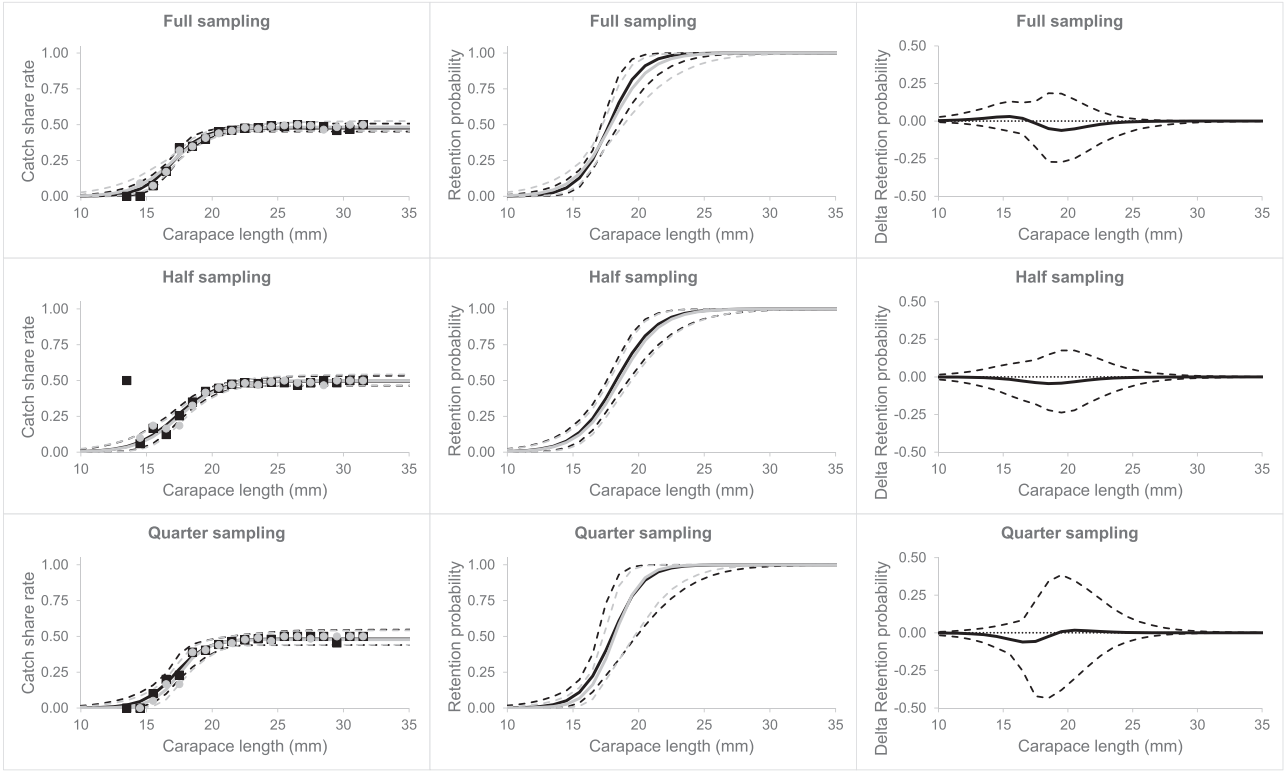

Fig. 13. Paired gear catch sharing data and curves (left) for a Nordmøre grid followed by a codend for manual data acquisition (black) and automatic acquisition (grey) at three sampling levels. Dots represent the experimental catch sharing rates. Full curves represent the estimated catch sharing rate curves, while dashed curves represent the CIs for the catch sharing rate. The centre column represents the size selection curves obtained from the sharing curves. The right column represents the delta curves (solid lines) with CIs (dashed lines) between size selection curves obtained using the automatic and manual data acquisition methods.

1996):

$$-\sum_{cl}\{nr_{cl}\times\ln(r(cl,\nu))+ne_{cl}\times\ln(1.0-r(cl,\nu))\} \tag{7}$$

Where the summation is over length classes in the data set.

In the case of the paired gear method, let nr_{cl} and nc_{cl} represent the number of shrimps of length class cl retained in the investigated gear and in the small mesh control gear towed parallel with the investigated gear, respectively. The parameters ν for the size selectivity curve model and the split parameter SP are then obtained by MLE minimizing:

$$-\sum_{cl}\left\{nr_{cl}\times\ln\left(\frac{SP\times r(cl,\nu)}{SP\times r(cl,\nu)+1.0-SP}\right)+nc_{cl}\times\ln\left(1.0-\frac{SP\times r(cl,\nu)}{SP\times r(cl,\nu)+1.0-SP}\right)\right\} \tag{8}$$

The split parameter SP quantifies the fraction of the shrimps entering the test gear, given that they enter one of the two gears (Wileman et al., 1996).

Besides absolute size selectivity, fishing gear scientists often estimate the relative length dependent catch efficiency (Krag et al., 2014). The data for this are often obtained by fishing the two gears simultaneously alongside each other to collect so-called catch comparison data (Grimaldo et al., 2016). In case of catch comparison data collection, the data consists of the length dependent number of shrimps, $nr1_{cl}$ and $nr2_{cl}$. These data are then used to estimate the parameters ν in the functional description of the catch comparison rate $cc(cl,\nu)$ by MLE minimizing:

$$-\sum_{cl}\{nr1_{cl}\times\ln(cc(cl,\nu))+nr2_{cl}\times\ln(1.0-cc(cl,\nu))\} \tag{9}$$

The catch comparison rate quantifies the length dependent probability of being captured in the first gear, given capture in one of the two gears (Herrmann et al., 2017). Therefore, for gear performance evaluation, $cc(cl,\nu)$ is often transformed to the catch ratio $cr(cl,\nu)$, which quantifies the length dependent relative capture probability between the two gears (Herrmann et al., 2017):

$$cr(cl,\nu)=\frac{cc(cl,\nu)}{1.0-cc(cl,\nu)} \tag{10}$$

The *Mdata* and *Adata* sets were used as entry data to simulate comparable datasets for absolute size selection. Like Section 2.7, we used the size selection curve for a Nordmøre grid with 19 mm bar spacing followed by a 35 mm diamond mesh codend (Larsen et al., 2017) to simulate the retained and released shrimps of the *Mdata* and *Adata* sets, using the same stochastic simulation approach as described above for the stock assessment evaluation. This lead to (nmr_{cl}, nmc_{cl}) and (nar_{cl}, nac_{cl}) to represent (nr_{cl}, nc_{cl}) in order to estimate the size selectivity curve $r(cl,\nu)$ by MLE by minimizing expression (7). For $r(cl,\nu)$, we tested two models, where the second, the double logistic *dlogistic*, was used in the simulations as this models the actual size selection process for such fishing gear configurations (Larsen et al., 2017):

$$\begin{aligned}&dlogistic\left(C_{grid},L50_{grid},SR_{grid},L50_{codend},SR_{codend},cl\right)\\&\quad=C_{grid}\times\left(1.0-logistic\left(L50_{grid},SR_{grid},cl\right)\right)\\&\qquad\times logistic\left(L50_{codend},SR_{codend},cl\right)\end{aligned} \tag{11}$$

The *dlogistic* model (11) is based on the *logistic* model often used to describe size selection in codends (Wileman et al., 1996):

$$logistic(L50,SR,cl)=\frac{\exp\left(\frac{\ln(2.0)}{SR}\times(cl-L50)\right)}{1.0+\exp\left(\frac{\ln(2.0)}{SR}\times(cl-L50)\right)} \tag{12}$$

Furthermore, as several other shrimp fisheries only use size selective codends (Einarsson et al., 2020), we also simulated that situation based

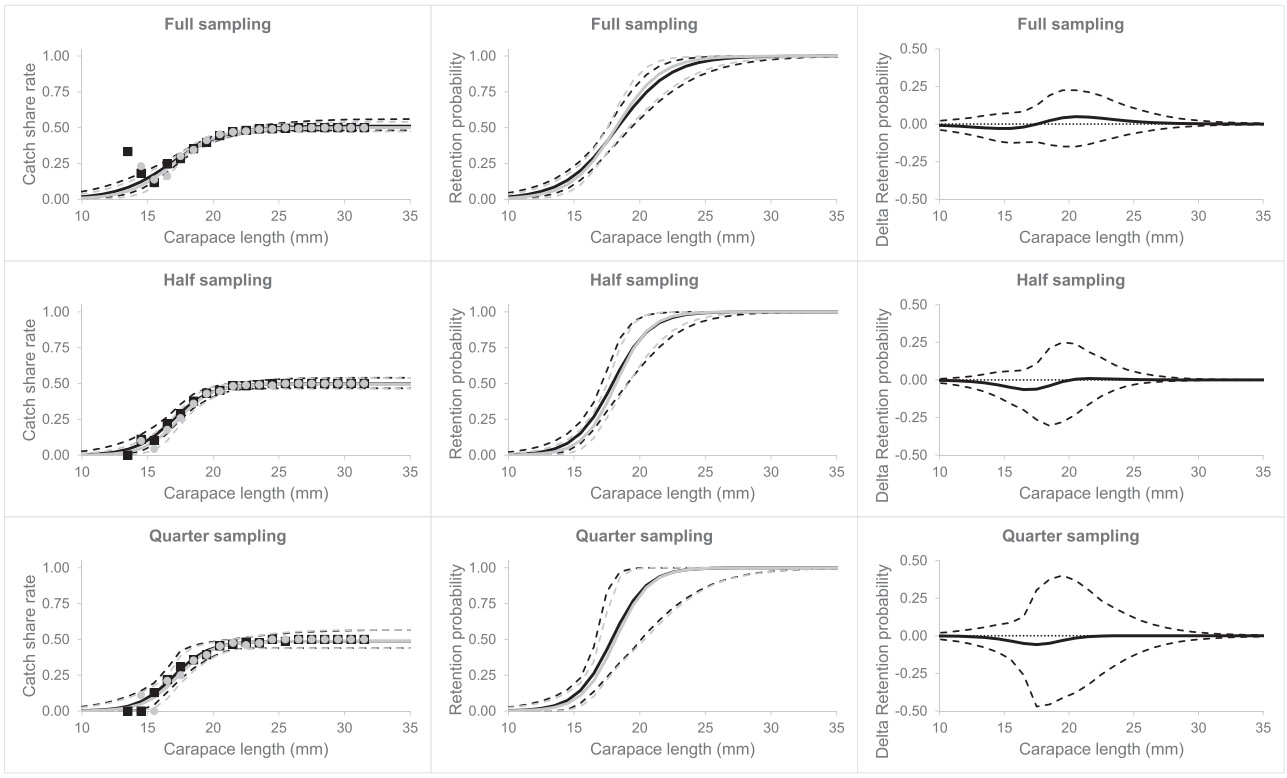

Fig. 14. Paired gear catch sharing data and curves (left) for the size-selective 35 mm mesh codend for manual data acquisition (black) and automatic acquisition (grey) at three sampling levels. Dots represent the experimental catch sharing rates. Full curves represent the estimated catch sharing rate curves, while dashed curves represent the CIs for the catch sharing rate. The centre column represents the size selection curves obtained from the sharing curves. The right column represents the delta curves (solid lines) with CIs (dashed lines) between size selection curves obtained using the automatic and manual data acquisition methods.

on the logistic model (12) using the codend size selection curve obtained by Larsen et al. (2017) for a 35 mm mesh size diamond mesh codend. For covered gear data, models (11) and (12) were used directly to simulate retained (nr_{cl}) and released (ne_{cl}) fractions, following the same approach as described above for simulating stock assessment data for a size selective fishing gear. For simulating paired gear data, the retained data (nr_{cl}) in the size selective gear was based on using (11) and (12) for $r(cl,\nu)$ dependent on if it was for nordmøre grid followed by codend or codend alone:

$$SP \times r(cl,\nu) \tag{13}$$

And for the retention in the nonselective gear (nc_{cl}):

$$1.0 - SP \tag{14}$$

For the simulations of the paired gear data using (13) and (14) with (11) or (12) the SP value was set at 0.5.

For the simulation of catch comparison data, we assumed a retention $r1(cl,\nu)$ for Nordmøre grid followed by a 35 mm mesh size diamond mesh codend modelled by (9) for gear one, and retention $r2(cl,\nu)$ for a 35 mm mesh codend modelled by (12) for gear two. Data were then simulated based on the results for deep-water shrimps obtained by Larsen et al. (2017). For gear one the retained data ($nr1_{cl}$) were simulated based on:

$$SP \times r1(cl,\nu) \tag{15}$$

And for gear two the retained data ($nr2_{cl}$) were simulated based on:

$$(1.0 - SP) \times r2(cl,\nu) \tag{16}$$

As with the stock assessment data, the comparison of results obtained from the simulated *Mdata* and *Adata* was done by analysing the delta for the size selection and catch ratio curves, respectively. This was accomplished by first using bootstrapping, following Herrmann et al. (2012), to obtain CIs for the individual curves. A significant difference between manual and automatic data collection methods was detected in cases where the CIs for the delta between curves did not contain the value 0.0.

2.8. Evaluation for fisheries management

In several fisheries, a central regulation is the establishment of a minimum legal size (MLS), and often a maximum limit is defined for the proportion of the catch that can consist of undersized individuals. deep-waterFor example, in the Norwegian shrimp fishery, a maximum of 10 % of the catch is allowed to be below MLS (Norwegian Directorate of Fisheries, 2011). If the fraction of the catch exceeds this limit, it leads to closure of the fishing grounds (Norwegian Directorate of Fisheries, 2011). The fraction of undersized individuals in a catch is often termed discard ratio (Wienbeck et al., 2014) and can, for deep-water shrimp, be given by:

$$nDRatio = \frac{\sum_{cl<MLS} n_{cl}}{\sum_{cl} n_{cl}} \tag{17}$$

We used the simulated retained part ($nr1_{cl}$) of the data covered gear size selection data described in Section 2.8 as input to (17) to obtain values for discard ratio for gear configurations for 19 mm Nordmøre grid followed by 35 mm mesh size diamond mesh codend, and this codend alone. For performance test purposes, we used a MLS set at 18 and 20 mm cl, respectively. Again, the delta between the results obtained from *Mdata* and *Adata* was used to assess the performance of the automatic data collection method.

2.9. Software

All simulations and analyses described in Sections 2.7–2.9 were

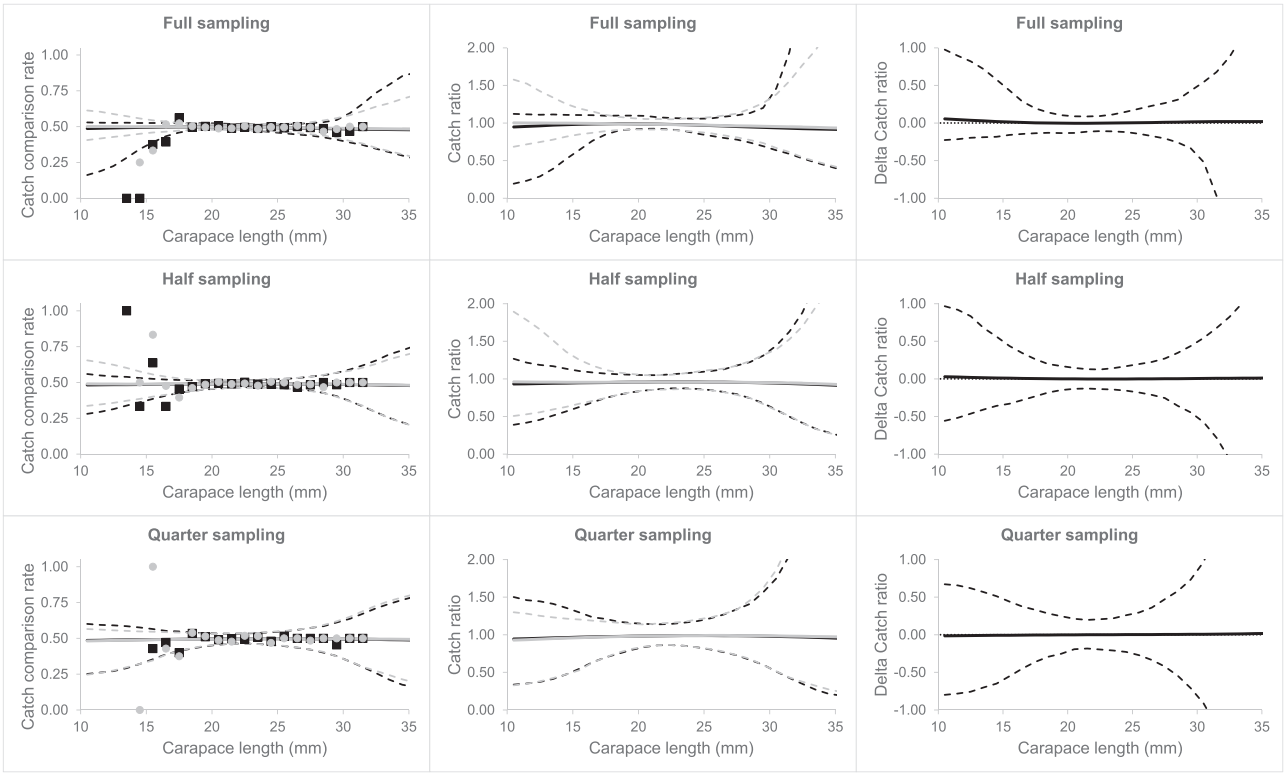

Fig. 15. Catch comparison data and curves (left) for a Nordmøre grid followed by a codend versus the codend alone for manual data acquisition (black) and automatic acquisition (grey) at three sampling levels. Dots represent the experimental catch comparison rates. Full curves represent the estimated catch comparison curves, while dashed curves represent the CIs for the catch comparison curves. The centre column represents the catch ratio curves obtained from the catch comparison curves. The right column represents the delta curves (solid lines) with CIs (dashed lines) between catch ratio curves obtained using the automatic and manual data acquisition methods.

Table 5
Discard ratios (%) obtained for manual automatic data acquisition methods for Nordmøre grid followed by codend and for codend alone. Numbers in () represents 95 % confidence bands. The delta column provides the difference between discard ratios obtained based on automatic and manual measured cl values for the shrimps.

Samling level	MLS	Grid + codend			Codend		
	(mm)	measured	estimated	delta	measured	estimated	delta
	18	7.8(6.9–8.7)	7.8(6.8–8.7)	0.0(−1.3–1.3)	7.4(6.4–8.4)	7.3(6.3–8.2)	−0.2(−1.7–1.1)
Full	20	22.9(21.6–24.2)	23.5(22.3–24.8)	0.6(−1.1–2.6)	22.4(21.1–23.7)	22.7(21.5–24.0)	0.4(−1.4–2.1)
	18	4.5(3.3–5.6)	3.7(2.7–4.8)	−0.7(−2.3–1.0)	5.3(4.1–6.5)	4.1(3.1–5.3)	−1.2(−2.8–0.5)
Half	20	16.2(14.6–17.7)	14.7(13.1–16.3)	−1.4(−3.7–0.7)	17.3(15.8–18.8)	15.8(14.3–17.3)	−1.5(−3.4–0.7)
	18	4.8(3.1–6.5)	3.3(1.8–4.9)	−1.5(−3.8–0.7)	6.2(4.2–8.1)	4.7(3.2–6.4)	−1.5(−3.8–1.1)
Quarter	20	16.3(14.0–18.6)	15.0(12.7–17.3)	−1.3(−4.3–1.9)	16.5(14.1–18.9)	15.0(12.8–17.5)	−1.5(−4.8–1.9)

carried out using the software tool SELNET (version date 6th April 2024) (Herrmann et al., 2012, 2016, 2022).

3. Results

3.1. Collection of shrimp data

A total of 2167 shrimp were sampled on the research vessel Helmer Hanssen. Deep-water shrimp was measured one by one, first manually and the immediately afterwards automatically. The measured size range for carapace length was 13.23 mm to 31.50 mm. Using the acquisition and image analysis described in Sections 2.2–2.3 2167 corresponding values for clm_i and vr_i were obtained and used to establish the values for parameters a and b in Eq. (2) (Fig. 5; Table 1). The corelation between *vs* and *clm* was strong, as the R^2-*value* for the fit was high (0.94).

3.2. Performance of automatic assessment on individual basis

Plotting *cla* against *clm* for the sampled shrimps showed the data centred around the baseline for zero deviation (Fig. 6, top panel). However, this plot also demonstrated some deviations, quantified by a mean absolute deviation at 0.55 mm, corresponding to a percentage deviation of 2.73 % (Table 2). The mean deviation is much smaller, with a value at 0.00023 mm, demonstrating that on a population basis, the automatic method provides a nearly unbiased value. However, the standard deviation is 0.72 mm, showing that predictions on single shrimp basis are not perfect. Nonetheless, the distribution of individual estimation deviations demonstrate that most are within ±2.5 mm (Fig. 6, centre panel) and within ±10 % (Fig. 6, lower panel).

3.3. Stock size structure assessment

The evaluation of the performance of the automatic measuring

method for stock assessment purposes was, as described in Section 2.7, based on comparing the population distributions of shrimp *cl* obtained from the *Mdata* (manually measured) and *Adata* (automatically measured). The frequency plots showed very similar distributions for the two methods for full, half, and quarter samplings, with overlapping CIs (Fig. 7, left column). This is further supported by the delta plots, which identified only one length class ($cl = 21.5$) where the CIs did not contain the baseline value of 0.0 for no difference in both full and half sampling, while no significant difference was observed for quarter sampling (Fig. 7, right column).

The frequency plots for comparing population size structures (Fig. 7) can be a bit noisy, and a less noisy comparison can often be obtained based on cumulative frequencies (Fig. 8). The results based on cumulative frequencies show very similar outcomes for the manual and automatic measurements of *cl* for shrimp (Fig. 8, left column), implying that the two acquisition methods lead to very similar results. This is supported by the delta plots (Fig. 8, right column), which showed the significant differences in cumulative frequences are only in the full sampling case, and only few length classes.

To further examine the performance of the automatic measuring method for stock assessment purposes, the *Mdata* and *Adata* sets were used to simulate the retained datasets with size-selective gear, specifically a 35 mm mesh diamond mesh codend, as described in Section 2.7. The performance on such "size-selected" data (Figs. 9–10) showed similarly good results for the automatic measuring method as for the non-size-selected data (Figs. 7–8), as the size frequency plots and cumulative size frequency plots exhibited very similar curves for the manual and automatic measuring of the shrimp.

3.4. Size selectivity assessment

The assessment of the performance of the automatic measuring method for estimating fishing gear size selectivity was conducted based on the simulation of size selectivity data using the *Mdata* and *Adata* for the covered gear, paired gear, and catch comparison data collection methods, following the procedures described in Section 2.8.

3.4.1. Covered gear analysis

For the simulated covered gear data for a Nordmøre grid followed by a size-selective codend and for the codend alone, we followed a standard analysis procedure by first using AIC values (Akaike, 1974) to determine which model to use for the data. In this case, both the *logistic* (Eq. 12) and the *dlogistic* (Eq. 11) models were considered (Table 3).

For the simulated covered gear data for a Nordmøre grid followed by a size-selective codend at all three sampling levels (full, half, and quarter), the analysis demonstrated that, despite some differences in the retention rate for individual data points obtained using the manual and automatic acquisition methods, the estimated selection curves appeared similar to each other (Fig. 11, left column). The exception was for the largest size classes of shrimp, where the CIs expanded for both data acquisition methods, leading to no significant differences in any size classes between the size selection curves. This is formally demonstrated by the delta plots, which show no significant differences between size selection curves obtained using the two sampling methods for any size classes of shrimp at any sampling level (Fig. 11, right column).

To further examine the performance of the automatic measuring method for estimating size selectivity from covered gear data, the *Mdata* and *Adata* sets were used to simulate the data obtained with size-selective gear, specifically a 35 mm diamond mesh codend, as described in Section 2.8. The performance based on those size selection data showed similarly good results for the automatic measuring method as the plots for the size selectivity are very similar for the manual and automatic measuring of the shrimp (Fig. 12, left column). This is collaborated by the delta plots, which show no significant differences between size selection curves obtained using the two sampling methods for any size classes of shrimp at any sampling levels (Fig. 12, right column).

3.4.2. Paired gear analysis

For the simulated paired gear data for a Nordmøre grid followed by a size-selective codend and for the codend alone, we followed a standard analysis procedure by first using AIC values to determine which model to use for the data. In this case, both the *logistic* (Eq. 12) and the *dlogistic* (Eq. 11) models were considered (Table 4).

The analysis at all three sampling levels (full, half, and quarter) demonstrated that, despite some differences in the catch sharing rate for individual data points obtained using the manual and automatic acquisition methods, the estimated catch share curves appeared very similar (Figs. 13 and 14, left column). Likewise, the estimated size selection curves seemed very similar for the two data acquisition methods (Figs. 13 and 14, centre column). This is formally demonstrated by the delta plots, which show no significant differences between size selection curves obtained using the two sampling methods for any size classes of shrimp at any sampling levels (Figs. 13 and 14, right column).

3.4.3. Catch comparison analysis

For the simulated catch comparison data for a Nordmøre grid followed by a size-selective codend versus the codend alone at all three sampling levels (full, half, and quarter), the analysis demonstrated that, despite some differences in the catch comparison rate for individual data points obtained using the manual and automatic acquisition methods, the estimated catch comparison curves appeared very similar (Fig. 15, left column). Likewise, the estimated catch ratio curves seemed very similar for the two data acquisition methods (Fig. 15, centre column). This is formally demonstrated by the delta plots, which show no significant differences between catch ratio curves obtained using the two sampling methods for any size classes of shrimp at any sampling levels (Fig. 15, right column).

3.5. Indicator assessment for fisheries management control of compliance

The assessment of the performance of the automatic measuring method for use in fisheries management control of compliance was conducted based on a simulation of the retained shrimp, using the *Mdata* and *Adata* following the procedures described in Section 2.9. The simulation was conducted for a Nordmøre grid followed by a size-selective codend versus the codend alone at three sampling levels (full, half, and quarter). The performance assessment was based on comparing the obtained discard ratios (Eq. 17), assuming MLS at 18 mm and 20 mm *cl*, respectively. The estimated discard ratios obtained very similar values for the two data acquisition methods across the cases investigated (Table 5). The delta values between manual and automatic measurements showed no significant difference between the two estimation methods was observed for any of the cases investigated (Table 5).

4. Discussion

In this study, we investigated whether an automatic method using computer vision and artificial intelligence for measuring the carapace length of deep-water shrimp can replace the current manual method using a calliper when data is used for stock assessment, fishing gear size selectivity estimation, or fisheries management purposes. Judging whether the automatic method provides sufficient accuracy to replace the current method for a specific purpose is challenging when based solely on comparing individual values for carapace length obtained with the two methods, as shown in Fig. 6 and Table 2. Therefore, we additionally employed what could be termed a use case-driven approach (Nebut et al., 2006). Specifically, we examined the consequences on the results in stock assessment, fishing gear size selectivity estimation, and fisheries compliance control if one or the other measuring method was used to obtain the dataset for the assessment. We compared results,

including considering the uncertainty in the results due to sample sizes, to evaluate whether applying one or the other measuring method led to significant differences in outcomes. For uncertainty estimation, we adopted the same methods commonly applied within the specific domain to make our assessment as realistic as possible. We believe that the outlined and applied use case-driven approach for evaluating whether a new measuring method can replace an existing one has advantages compared to judging based on single sample measures, as provided in Fig. 6 and Table 2, a method often used (Lai et al., 2022; Monkman et al., 2019).

Based on our use case-driven approach, we found that an automatic measuring procedure based on "off-the-shelf" camera technology combined with a general-purpose artificial intelligence algorithm can provide sufficient accuracy to replace manual measurement of deep-water shrimp for data use in stock assessment, gear size selectivity, and compliance control assessment purposes, despite some deviations in individual shrimp size measurements between the manual and automatic methods (Fig. 6; Table 2). If we had based the evaluation solely on a non-use case-driven approach like Fig. 6 and Table 2, we would not have been able to determine whether the automatic method provided sufficient accuracy to replace the manual method. This demonstrates the usefulness of adopting a use case-driven approach for the performance evaluation of a new measuring technique, as done in this study.

The manual measurement of the size of deep-water shrimp with a calliper is a direct measuring procedure of the attribute of interest (here, the carapace length). However, automatically identifying and locating the two endpoints defining the carapace length on every image (Fig. 1) can be challenging. Therefore, for our computer vision-based method, we used an indirect approach by utilizing a strong correlation between the shrimp volume *vr* and the carapace length, as given by Eq. (2). In this respect, our measurement approach has some similarities with the method investigated by Harbitz (2007), who based the estimation on a correlation between shrimp area and carapace length. Despite the issue with the side of the shrimp facing away from the camera that is obscured in our acquisition method, we believe that using volume *vr* instead of, for example, area provides a more robust measurement regarding segmentation errors (separating the shrimp from the background). Compared to area measurement, where each segmented pixel contributes equally to the area sum, a pixel in the centre of the shrimp contributes more to the total volume due to its height measurement, than an erroneously segmented pixel at the border of the shrimp, e.g., segmentation of its whiskers. However, future work could compare these two methods in detail. Other examples of using artificial intelligence in combination with computer vision to assess shrimp size by means of other estimation procedures include Lin et al. (2019) and Setiawan et al. (2022).

Our study is another example of how modern technology, in this case based on computer vision and artificial intelligence, provides new possibilities for data sampling and processing in marine science applications, aligning with the objectives of the working group WGLEARN (ICES, 2019). A comprehensive reference list of works and methods for marine applications of artificial intelligence can be found in Rubbens et al. (2023).

CRediT authorship contribution statement

Anja Helene Alvestad: Writing – original draft, Project administration, Investigation, Data curation. **Elling Ruud Øye:** Writing – original draft, Visualization, Validation, Resources, Methodology, Investigation, Formal analysis, Data curation, Conceptualization. **Jonatan Sjølund Dyrstad:** Writing – original draft, Validation, Resources, Methodology, Investigation, Conceptualization. **Bent Herrmann:** Writing – original draft, Visualization, Validation, Software, Methodology, Investigation, Funding acquisition, Formal analysis, Conceptualization.

Declaration of Competing Interest

The authors declare that they have no known competing financial interests or personal relationships that could have appeared to influence the work reported in this paper.

Data Availability

Data will be made available on request.

Acknowledgements

We thank the crew of the R/V Helmer Hanssen for their valuable assistance on board the vessel. We acknowledge the help from Jørgen Vollstad from Sintef Ocean during the data collection. We are grateful for financial support from the Research Council of Norway through grant number 320822 ("R-control: Technology for effective and sustainable resource control"). Finally, we express our gratitude to the two reviewers for their valuable comments, which helped improving our manuscript significantly.

References

Akaike, H., 1974. A new look at the statistical model identification. IEEE Trans. Auto. Control 19, 716–722. https://doi.org/10.1109/TAC.1974.1100705.

Alvarez-Ellacuría, A., Palmer, M., Catalá, n, I.A., Lisani, J.-L., 2020. Image-based, unsupervised estimation of fish size from commercial landings using deep learning. ICES J. Mar. Sci. 77, 1330–1339. https://doi.org/10.1093/icesjms/fsz216.

Duarte, C.M., Agusti, S., Barbier, E., Britten, G.L., Castilla, J.C., Gattuso, J.-P., et al., 2020. Rebuilding marine life. Nature 580, 39–51. https://doi.org/10.1038/s41586-020-2146-7.

Efron, B., 1982. The jackknife, the bootstrap and other resampling plans. In: SIAM Monograph No. 38; CBSM-NSF Regional Conference Series in Applied Mathematics. Philadelphia, ISBN 978-0-89871-179-0. https://doi.org/10.1137/1.9781611970319.

Einarsson, H.A., Chen, Z., Bayse, S., Herrmann, B., Winger, P., 2020. Comparing the size selectivity of a novel T90 mesh codend to two conventional codends in the Northern shrimp (*Pandalus borealis*) trawl fishery. Aquac. Fish. https://doi.org/10.1016/j.aaf.2020.09.005.

Fischler, M.A., Bolles, R.C., 1981. Random sample consensus: a paradigm for model fitting with applications to image analysis and automated cartography. Commun. ACM 24, 381–395. https://doi.org/10.1145/358669.358692.

Grimaldo, E., Sistiaga, M., Herrmann, B., Larsen, R.B., 2016. Trawl Selectivity in the Barents Sea Demersal Fishery. Chapter in: Fisheries and Aquaculture in the Modern World. DOI: 10.5772/63019.

Harbitz, A., 2007. Estimation of shrimp (*Pandalus borealis*) carapace length by image analysis. ICES J. Mar. Sci. 64, 939–944.

Hashisho, Y., Dolereit, T., Segelken-Voigt, A., Bochert, R., Vahl, M., 2021. AI-assisted Automated Pipeline for Length Estimation, Visual Assessment of the Digestive Tract and Counting of Shrimp in Aquaculture Production. In Proceedings of the 16th International Joint Conference on Computer Vision, Imaging and Computer Graphics Theory and Applications (VISIGRAPP 2021) - Volume 4: VISAPP, pages 710-716, ISBN: 978-989-758-488-6. DOI: 10.5220/0010342007100716.

Herrmann, B., Sistiaga, M., Nielsen, K.N., Larsen, R.B., 2012. Understanding the size selectivity of redfish (*Sebastes spp.*) in North Atlantic trawl codends. J. Northwest Atl. Fish. Sci. 2012 (44), 1–13. https://doi.org/10.2960/J.v44.m68.

Herrmann, B., Sistiaga, M., Santos, J., Sala, A., 2016. How many fish need to be measured to effectively evaluate trawl selectivity? PLoS ONE 11 (8), e0161512. https://doi.org/10.1371/journal.pone.0161512.

Herrmann, B., Sistiaga, M., Rindahl, L., Tatone, I., 2017. Estimation of the effect of gear design changes on catch efficiency: methodology and a case study for a Spanish longline fishery targeting hake (*Merluccius merluccius*). Fish. Res. 2017 (185), 153–160. https://doi.org/10.1016/j.fishres.2016.09.013.

Herrmann, B., Krag, L.A., Krafft, B.A., 2018. Size selection of Antarctic krill (*Euphausia superba*) in a commercial codend and trawl body. Fish. Res. 207, 49–54. https://doi.org/10.1016/j.fishres.2018.05.028.

Herrmann, B., Cerbule, K., Brčić, J., Grimaldo, E., Geoffroy, M., Daase, M., Berge, J., 2022. Accounting for uncertainties in biodiversity estimations: a new methodology and its application to the mesopelagic sound scattering layer of the high Arctic. Front. Ecol. Evol. 2022 (10), 775759. https://doi.org/10.3389/fevo.2022.775759.

ICES, 2019. Working group on machine learning in marine science (WGMLEARN). ICES Sci. Rep. 1 (45), 13. https://doi.org/10.17895/ices.pub.5539.

Jardim, E., Azevedo, M., Brites, N.M., 2015. Harvest control rules for data limited stocks using length-based reference points and survey biomass indices. Fish. Res. 171, 12–19. https://doi.org/10.1016/j.fishres.2014.11.013.

Jennings, S., Kaiser, M.J., 1998. The effects of fishing on marine ecosystems. In: Blaxter, J.H.S., Southward, A.J., Tyler, P.A. (Eds.), Advances in Marine Biology. Academic Press, pp. 201–352 (Eds).

Jennings, S., and Polunin, N.V.C., 1997. Impacts of predator depletion by fishing on the biomass and diversity. https://doi.org/10.1007/s003380050061.

Kennelly, S.J., Broadhurst, M.K., 2021. A review of bycatch reduction in demersal fish trawls. Rev. Fish. Biol. Fish. 31, 289–318. https://doi.org/10.1007/s11160-021-09644-0.

Krag, L.A., Herrmann, B., Karlsen, J., 2014. Inferring fish escape behaviour in trawls based on catch comparison data: model development and evaluation based on data from Skagerrak, Denmark. pmid:24586403. PLoS One 9 (2), e88819. https://doi.org/10.1371/journal.pone.0088819.

Lai, P.C., Lin, H.Y., Lin, J.Y., Hsu, H.C., Chu, Y.N., Liou, C.H., Kuo, Y.F., 2022. Automatic measuring shrimp body length using CNN and an underwater imaging system. Biosyst. Eng. 221, 224–235. https://doi.org/10.1016/j.biosystemseng.2022.07.006.

Larsen, R.B., Herrmann, B., Sistiaga, M., Brinkhof, J., Tatone, I., Langård, L., 2017. Performance of the Nordmøre grid in shrimp trawling and potential effects of guiding funnel length and light stimulation. Mar. Coast. Fish. Dyn. Manag. Ecosyst. Sci. 9, 479–492. https://doi.org/10.1080/19425120.2017.1360421.

Larsen, R.B., Herrmann, B., Sistiaga, M., Brčić, J., Brinkhof, J., Tatone, I., 2018a. Could green artificial light reduce bycatch during Barents Sea deep-water shrimp trawling? Fish. Res. 204, 441–447. https://doi.org/10.1016/j.fishres.2018.03.023.

Larsen, R.B., Herrmann, B., Sistiaga, M., Brinkhof, J., Grimaldo, E., 2018b. Bycatch reduction in the Norwegian deep-water shrimp (Pandalus borealis) fishery with a double grid selection system. Fish. Res. 208, 267–273. https://doi.org/10.1016/j.fishres.2018.08.007.

Lin, H.Y., Lee, H.C., Ng, W.L., Pai, J.N., Chu, Y.N., Liou, C.H., Liao, K.C., Kuo, Y.F., 2019. Estimating shrimp body length using deep convolutional neural network. 2019 ASABE Annual International Meeting. American Society of Agricultural and Biological Engineers. https://doi.org/10.13031/aim.201900724.

Marrable, D., Barker, K., Tippaya, S., Wyatt, M., Bainbridge, S., Stowar, M., et al., 2022. Accelerating species recognition and labelling of fish from underwater video with machine-assisted deep learning. Front. Mar. Sci. 9. https://doi.org/10.3389/fmars.2022.944582Marrable2022.

Marrable, D., Tippaya, S., Barker, K., Harvey, E., Bierwagen, S.L., Wyatt, M., Bainbridge, S., Stowar, M., 2023. Generalised deep learning model for semi-automated length measurementof fish in stereo-BRUVS. Front. Mar. Sci. 10, 1171625. https://doi.org/10.3389/fmars.2023.1171625.

Melnychuk, M.C., Kurota, H., Mace, P.M., Pons, M., Minto, C., Osio, G.C., et al., 2021. Identifying management actions that promote sustainable fisheries. Nat. Sustain. 4, 440–449. https://doi.org/10.1038/s41893-020-00668-1.

Monkman, G.G., Hyder, K., Kaiser, M.J., Vidal, F.P., 2019. Using machine vision to estimate fish length from images using regional convolutional neural networks. Methods Ecol. Evol. 10, 2045–2056. https://doi.org/10.1111/2041-210X.13282.

Mytilineou, C., Herrmann, B., Kavadas, S., Megalofonou, P., Somarakis, S., 2020. Combining selection models and population structures to inform fisheries management: a case study on hake in the Mediterranean bottom trawl fishery. Mediterr. Mar. Sci. 21 (2), 360–371. https://doi.org/10.12681/mms.22191.

Nebut, C., Fleurey, F., Le Traon, Y., Jezequel, J.M., 2006. Automatic test generation: a use case driven approach. IEEE Trans. Softw. Eng. VOL. 32 (NO. 3). https://doi.org/10.1109/TSE.2006.2.

Norwegian Directorate of Fisheries. 2011. J-209-2011: forskrift om maskevidde, bifangst og minstemål m.m. ved fiske i fiskevernsonen ved Svalbard. (In Norwegian). ⟨https://lovdata.no/dokument/SF/forskrift/1994-09-21-881#KAPITTEL_2⟩. (October 2017).

Pauly, D., Christensen, V., Guénette, S., Pitcher, T.J., Sumaila, U.R., Walters, C.J., et al., 2002. Towards sustainability in world fisheries. Nature 418, 689–695. https://doi.org/10.1038/nature01017.

Rubbens, P., Brodie, S., Cordier, T., Barcellos, D.D., Devos, P., Fernandes-Salvador, J.A., Fincham, J.I., Gomes, A., Handegard, N.O., Howell, K., Jamet, C., Kartveit, K.H., Moustahfid, H., Parcerisas, C., Politikos, D., Sauzède, R., Sokolova, M., Uusitalo, L., Van den Bulcke, L., van Helmond, A.T.M., Watson, J.T., Welch, H., Beltran-Perez, O., Chaffron, S., Greenberg, D.S., Kühn, B., Kiko, R., Lo, M., Lopes, R.M., Möller, K.O., Michaels, W., Pala, A., Romagnan, J.-B., Schuchert, P., Seydi, V., Villasante, S., Malde, K., Irisson, J.-O., 2023. Machine learning in marine ecology: an overview of techniques and applications. ICES J. Mar. Sci. Volume 80 (Issue 7), 1829–1853. https://doi.org/10.1093/icesjms/fsad100.

Setiawan, A., Hadiyanto, H., Widodo, C.E., 2022. Shrimp body weight estimation in aquaculture ponds using morphometric features based on underwater image analysis and machine learning approach. Rev. D. 'Intell. Artif. 36, 905–912. https://doi.org/10.18280/ria.360611.

Silva, C.S., Aires, R., Rodrigues, F., 2020. Automatic fish measurement using a camera and a 3D sensor applied to a long-term experiment. ICES J. Mar. Sci. 77, 3050–3057. https://doi.org/10.1093/icesjms/fsaa190.

White, D.J., Svelling, C., Strachan, N.J.C., 2006. Automated measurement of species and length of fish by computer vision. Fish. Res. 80, 203–210. DOI: 10.1016j.fishres.2006.04.009.

Wienbeck, H., Herrmann, B., Feekings, J.P., Stepputtis, D., Moderhak, W., 2014. Fish. Res. 2014 (150), 28–37. https://doi.org/10.1016/j.fishres.2013.10.007.

Manual of Methods of Measuring the Selectivity of Towed Fishing Gears. In: Wileman, D. A., Ferro, R.S.T., Fonteyne, R., Millar, R.B. (Eds.), 1996. ICES Coop. Res. Rep. No. 215, ICES, Copenhagen, Denmark.